Journal of Power Sources 188 (2009) 96–105

Contents lists available at ScienceDirect

Journal of Power Sources

journal homepage: www.elsevier.com/locate/jpowsour

Intermediate-temperature electrochemical performance of a polycrystalline $PrBaCo_2O_{5+\delta}$ cathode on samarium-doped ceria electrolyte

Dengjie Chen, Ran Ran, Kun Zhang, Jun Wang, Zongping Shao*

State Key Laboratory of Materials-Oriented Chemical Engineering, College of Chemistry & Chemical Engineering, Nanjing University of Technology, No. 5 Xin Mofan Road, Nanjing 210009, PR China

ARTICLE INFO

Article history:
Received 25 September 2008
Received in revised form
14 November 2008
Accepted 14 November 2008
Available online 21 November 2008

Keywords:
Solid-oxide fuel cells
Impedance spectroscopy
Mixed conductor
$PrBaCo_2O_{5+\delta}$
Cathode

ABSTRACT

A-site cation-ordered $PrBaCo_2O_{5+\delta}$ (PrBC) double perovskite oxide was synthesized and evaluated as the cathode of an intermediate-temperature solid-oxide fuel cell (IT-SOFC) on a samarium-doped ceria (SDC) electrolyte. The phase reaction between PrBC and SDC was weak even at 1100 °C. The oxygen reduction mechanism was investigated by electrochemical impedance spectroscopy characterization. Over the intermediate-temperature range of 450–700 °C, the electrode polarization resistance was mainly contributed from oxygen-ion transfer through the electrode–electrolyte interface and electron charge transfer over the electrode surface. An area-specific resistance as low as ~0.4 $\Omega\,cm^2$ was measured at 600 °C in air, based on symmetric cell test. A thin-film SDC electrolyte fuel cell with PrBC cathode was fabricated which delivered attractive peak power densities of 620 and 165 $mW\,cm^{-2}$ at 600 and 450 °C, respectively.

1. Introduction

Solid-oxide fuel cells (SOFCs) have received tremendous attention recently due to their high-energy conversion efficiency, low emissions and excellent fuel flexibility. Traditional SOFCs are based on yttria-stabilized zirconia electrolyte and typically operated at ~1000 °C to ensure affordable power density. Nowadays, there is great interest in reducing the operation temperature of SOFCs to the intermediate range of 500–800 °C for couple of benefits associated with such temperature reduction, for example versatile cell materials, prolonged lifetime, elegant sealing, and reduced fabrication cost [1,2]. However, rapid deterioration of cathode performance with the drop of operation temperature has become a major obstacle for the development of intermediate-temperature (IT)-SOFCs. Traditional SOFC cathodes are composed of $La_{0.8}Sr_{0.2}MnO_3$ perovskite-type oxide [3,4], which is a pure electronic conductor under zero direct current passage with oxygen reduction strictly limited to the electrolyte–electrode–air triple-phase boundary (TPB). Recently, mixed ionic and electronic conducting (MIEC) oxides have received tremendous attention as potential cathodes of IT-SOFCs [5–15]. Since the oxygen-ion conduction can penetrate into the electrode bulk, the active sites for oxygen reduction are greatly extended; consequently, interfacial polarization is obviously improved at reduced temperatures by using a MIEC cathode.

Most MIEC electrode materials have a perovskite-type lattice structure [8–15], in which the oxygen-ion can migrate in all three dimensions. More recently, a new type of MIEC oxides, i.e. cation-ordered $LnBaCo_2O_{5+\delta}$ (Ln = Gd, Pr, Y, La, etc.), with two dimensional ion diffusion channels have attracted much interest [16–26]. The crystal structure of these oxides can be regarded as a layered crystal $A'A''B_2O_6$ by doubling the unit cell of the standard perovskite structure, and consists of consecutive layers $[BO_2]$–$[A''O]$–$[BO_2]$–$[A'O_\delta]$ stacked along the *c*-axis [21]. The transformation of a cubic perovskite to such a layered structure reduces the oxygen bonding strength in the $A'O_\delta$ layer and provides disorder-free channels for ion motion [16], which remarkably enhances oxygen diffusivity and opens the possibility for developing a new class of materials suitable for SOFC cathodes.

Among the various $LnBaCo_2O_{5+\delta}$ oxides, $GdBaCo_2O_{5+\delta}$ (GdBC) has been the most investigated [22–25]. Recently, its performance as a cathode of IT-SOFCs on proton-conducting $BaZr_{0.1}Ce_{0.7}Y_{0.2}O_3$ electrolytes, $Sm_{0.2}Ce_{0.8}O_{1.9}$ (SDC) and yttria-stabilized zirconia has been explored [22–24]. By applying electrical conductivity relaxation techniques, Jacobson and co-workers demonstrated that bulk diffusion coefficient and surface exchange coefficient for $PrBaCo_2O_{5+\delta}$ (PrBC) could be 2–3 orders of magnitude higher than the values reported for GdBC [21], suggesting it may perform even better than GdBC as a cathode of IT-SOFCs. Their primary experi-

* Corresponding author. Tel.: +86 25 83172256; fax: +86 25 83365813.
E-mail addresses: theretheir@sina.com (D. Chen), ranrandalian@yahoo.com (R. Ran), sun_rain518@163.com (K. Zhang), junwang@njut.edu.cn (J. Wang), shaozp@njut.edu.cn (Z. Shao).

0378-7753/$ – see front matter © 2008 Elsevier B.V. All rights reserved.
doi:10.1016/j.jpowsour.2008.11.045

mental results show that an area specific resistance (ASR) as low as ~0.15 Ω cm^2 at 600 °C can be achieved by applying a mixture of PrBC and Gd_2O_3-doped CeO_2 as the cathode on a Gd_2O_3-doped CeO_2 electrolyte [21].

To optimize the performance of a cathode, it is crucial to know the mechanism and kinetics of the oxygen reduction reaction. Up to now, such information is still lack in the literature regarding PrBC electrodes. In this study, PrBC was synthesized by a sol–gel technique. Electrochemical impedance spectroscopy (EIS) techniques have been applied to investigate its activity for oxygen reduction based on symmetric cell configuration. Complete cells with PrBC cathode on SDC electrolyte were also fabricated and evaluated. High performance was achieved.

2. Experimental

2.1. Powder synthesis and cell fabrication

Both PrBC oxide and SDC oxide powders were synthesized by a combined EDTA–citrate complexing sol–gel process [27,28]. The synthesis of PrBC, as an example, is described as follows. $Pr(NO_3)_3$, $Ba(NO_3)_2$ and $Co(NO_3)_2$, all in analytical grade, were applied as the raw materials of cations. Stoichiometric amounts of the above metal nitrates according to the molecular composition $PrBaCo_2O_{5+\delta}$ were prepared into a mixed solution. EDTA-$NH_3{\cdot}H_2O$ and citric acid were added in sequence at a mole ratio of 1:1:2 for total metal ions:EDTA:citric acid under heating and stirring. A transparent gel was obtained by evaporating the water from the solution that was pre-fired to 250 °C to solidify the gel and followed by calcination at 950–1000 °C for 5 h in air to obtain the final product with the desired lattice structure.

For fabricating symmetric cells, the as-prepared SDC powder was pressed into disk-shaped pellets using a 15 mm diameter stainless steel die under a hydraulic pressure of 10 MPa, followed by sintered at 1450 °C for 5 h in air. The resulted dense pellets have a diameter of ~13.0 mm and thickness of ~1.0 mm. To prepare the electrode layers, PrBC oxide (well dispersed in a mixed solution of ethylene glycol, ethanol and isopropyl alcohol) was symmetrically deposited onto both surfaces of the electrolytes by spray, followed by calcination at 1000 °C for 5 h. The obtained cells with symmetric PrBC electrodes were then used for EIS measurement.

Anode-supported thin-film SDC electrolyte cells were fabricated by a dual dry pressing followed by sintered at 1450 °C for 5 h in air. A NiO + SDC mixture, prepared by mixing SDC powder and NiO in a 40/60 weight ratio, was pressed into pellets using a 15 mm stainless steel die. The proper amount of SDC powder, prepared by the EDTA–citrate complexing method, was dispersed homogeneously over the open surface of the anode pellets inside the die and pressed again to form dual layer green pellets. These green cells were then sintered at 1450 °C for 5 h in air to densify the electrolyte layer. The PrBC suspension was then spray deposited over the other electrolyte surface, followed by calcination at 1000 °C for 5 h in air. The three-layered pellets were then used for *I–V* characterization.

2.2. Characterization

The phase structure of synthesized powders was characterized with an X-ray diffractometer (XRD, Bruker D8 Advance) equipped with Cu Kα radiation (λ = 1.5418 Å). The reactivity of PrBC with SDC was investigated by mixing and grinding the two powders in a 50/50 weight ratio and calcinated at various temperatures in the range of 900–1100 °C at 50 °C intervals. Microscopic features of the symmetric cells and the three-layered single cells were characterized using a scanning electron microscope (SEM, Hitachi-X650).

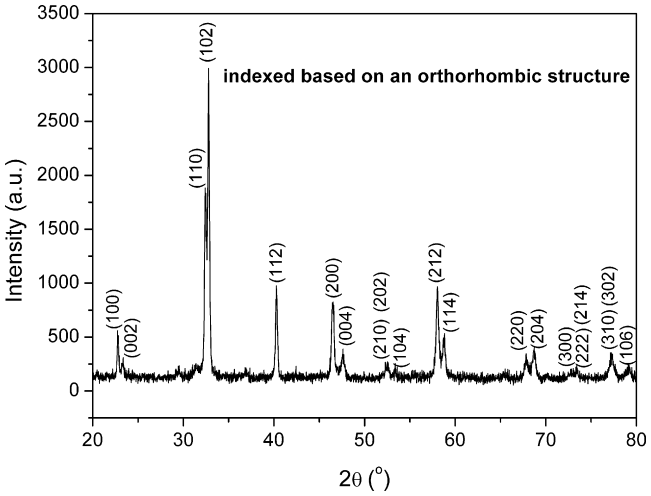

Fig. 1. Room-temperature XRD pattern of $PrBaCo_2O_{5+\delta}$ oxide after calcination at 950 °C in air for 5 h.

Both electrode surfaces of the symmetric cells were painted with a thin layer of silver to act as current collectors. The cell was then loaded into a quartz tube reactor with controllable atmosphere for electrochemical impedance spectra (EIS) measurement using a Solartron 1260 Frequency Response Analyzer in combination with a Solartron 1287 potentiostat. The frequency used for EIS measurements ranged from 10^{-1}–10^{-2} to 10^5–10^6 Hz with a signal amplitude of 10 mV. Samples were tested under open circuit voltage (OCV) condition. The oxygen partial pressure of the atmosphere was varied between 0.04 and 1 atm by mixing O_2 with N_2 using mass flow controllers. The 3 vol.% water vapor was introduced by bubbling gas through a water bottle at 25 °C.

The fuel cell test was performed in an in-lab constructed SOFC test station. The cell was sealed onto the top of a quartz tube with the cathode side and anode side flowing with dry or humidified air at 300 ml min^{-1} [STP] and hydrogen at 80 ml min^{-1} [STP], respectively. A Keithley 2420 source meter was used for *I–V* polarization tests. A four-terminal configuration was employed. The cell impedance under OCV condition was also measured.

3. Results and discussion

3.1. Optimizing the firing temperature

Fig. 1 shows the room-temperature X-ray diffraction patterns of the PrBC oxide prepared by the combined EDTA–citrate complexing method after calcination at 950 °C for 5 h. All the diffraction peaks can be indexed well based on an orthorhombic structure, space group *Pmmm*, and the unit cell parameters a = 3.9041 Å, b = 3.9048 Å, c = 7.6358 Å, which are in good agreement with literature results [21,29]. It suggests that the layered perovskite structure is well developed after the calcination.

It is well known that SOFC electrode performance is closely related with many factors, such as its phase structure, its electrical conductivity, the phase reaction between electrode and electrolyte, and the physical connection between the electrode and electrolyte layers. The phase reaction between electrode and electrolyte may create an insulating interfacial layer and block oxygen transfer from the electrode to the electrolyte [30] while a poor connection between electrolyte and electrode layers would result in large contact resistance. The reactivity between PrBC and SDC was investigated by mixing them in powder state in a 50/50 weight ratio followed by calcination in air between 900 and 1100 °C for 5 h. The corresponding X-ray diffraction patterns of the mixed powder after

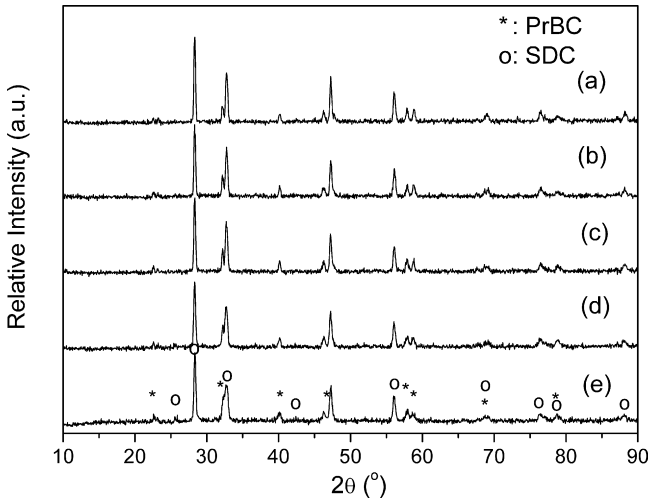

Fig. 2. XRD patterns of the $PrBaCo_2O_{5+\delta}$–SDC mixture after calcination at various temperatures in air for 5 h: (a) 1100 °C, (b) 1050 °C, (c) 1000 °C, (d) 950 °C and (e) 900 °C.

the calcinations are shown in Fig. 2. Within the investigated temperature range, all the diffraction peaks could be indexed well based on a physical mixture of PrBC and SDC phases, and the unit cell parameters of SDC from 900 to 1000 °C are a_{900} = 5.4370 Å, a_{950} = 5.4412 Å, a_{1000} = 5.4375 Å, a_{1050} = 5.4389 Å and a_{1100} = 5.4367 Å, which vary slightly at different temperature and are in good agreement with the value (JCPDS Card Number 75-0158). It suggests that no serious reaction between these two components. Since the high temperature calcinations result in electrode sintering, a lower firing temperature is preferred. However, a certain degree of solid-state reaction between the electrolyte and electrode layer is necessary to ensure a good connection. A firing temperature of 1000 °C was adopted for the PrBC cathode layer.

As shown in Fig. 3 are the cross-sectional morphologies of a complete cell (Fig. 3a) and a symmetric cell (Fig. 3b) with PrBC electrode(s), which were fabricated onto the electrolyte surface by firing at 1000 °C for 5 h. It demonstrated that the PrBC electrode adhered to the electrolyte surface pretty well with no any delamitation observed. The well-developed connections between the two layers then ensure a low contact resistance. Furthermore, no observable interfacial layer between PrBC and SDC electrolyte was detected, agreeing well with the XRD results. In the following results, a firing temperature of 1000 °C was adopted for fabricating the PrBC electrode layer.

3.2. Oxygen reduction mechanism

The overall electrochemical reaction for oxygen reduction at a SOFC cathode can be simply described as follows:

$$\frac{1}{2}O_2(g) + 2e^- = O^{2-} \quad (1)$$

In reality, it may involve many sub-steps such as gas diffusion, surface adsorption, dissociation, electron and ion charge transfer, and so on. It is of vital importance to have mechanistic and kinetic knowledge of the oxygen reduction at the cathode to improve cell performance. To get such information, complex impedance measurements of the single-phase PrBC electrode on the SDC electrolyte were collected every 50 °C in the temperature range from 450 to 700 °C. Experimental data in Nyquist plots and fitting results for a symmetrical PrBC/SDC/PrBC cell measured at open circuit in air are presented in Fig. 4. In general, the spectra measured include a high-frequency induction tail ascribed to the device and connect leads. In the temperature range 450–550 °C, two well-separated semi-circles were observed in the Nyquist plots. With increasing operating temperature, the high-frequency arc size decreased noticeably, and the arc was totally disappeared at 600 °C and higher. An additional arc at the low frequency range ($1–10^{-1}$ Hz) appeared when the operating temperature was elevated to 700 °C.

It was found that the EIS data for a PrBC/SDC/PrBC symmetric cell can be fitted well to the equivalent circuit L–R_b–(R–C)–(R_1-QPE_1)–(R_2-QPE_2)...(R_i-QPE_i). The appearance of R–C impedance (made by a resistor R in parallel with capacitor) and the number of R_i-QPE_i impedances (made by a resistor R_i in parallel with a constant phase element QPE_i) in series are dependent on operation temperature. The exact equivalent circuits adopted for fitting the EIS data at various temperatures are presented inside the Nyquist plots in Fig. 4. The impedances of a symmetric cell may arise from both the electrodes and electrolyte. The electrolyte typically performs as an ideal resistor and displays only a dot in the Nyquist plots at high temperatures in the investigated frequency range of 10^6–10^{-2} Hz. However, with the decrease in operation temperature, a semi-circle associated with the oxide-ion diffusion around the grain boundary of the electrolyte also appeared in the high-frequency range. For example, Zhan et al. observed that the arc associated with the grain boundary ionic diffusion appeared at an operation temperature of 460 °C in the complex impedance plane plots [31]. It was found that the EIS data for the PrBC/SDC/PrBC symmetric cell at 450 °C can be fitted well to an equivalent circuit of L–R_b–(R–C)–(R_1-QPE_1)–(R_2-QPE_2)–(R_3-QPE_3). The semi-circle at the high-frequency

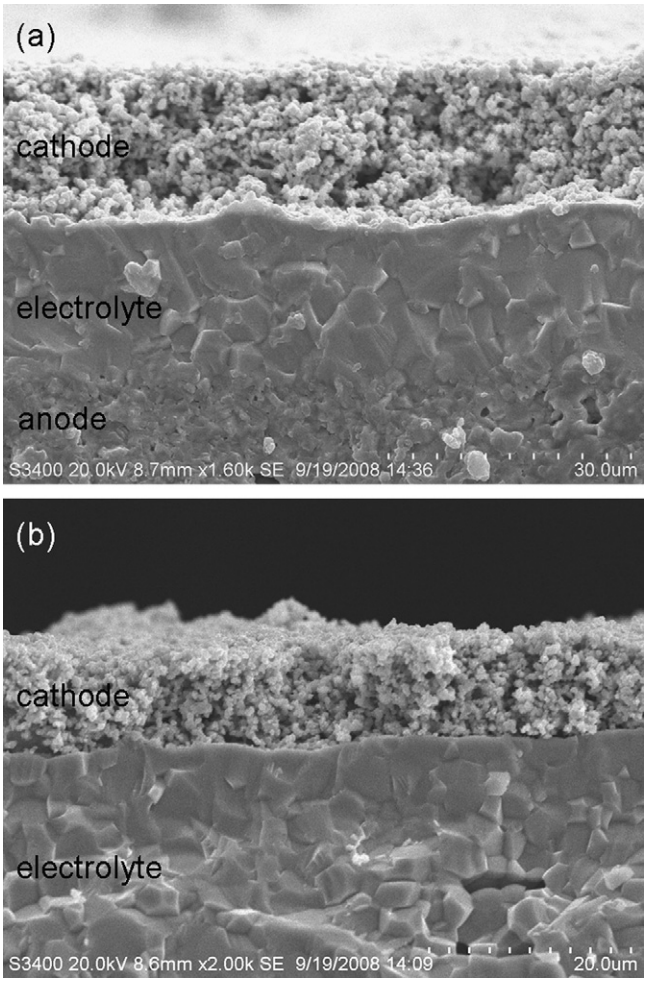

Fig. 3. SEM photos of the cross-sectional view of (a) a complete fuel cell with PrBC cathode and (b) an interface between PrBC electrode and SDC electrolyte for a symmetric cell.

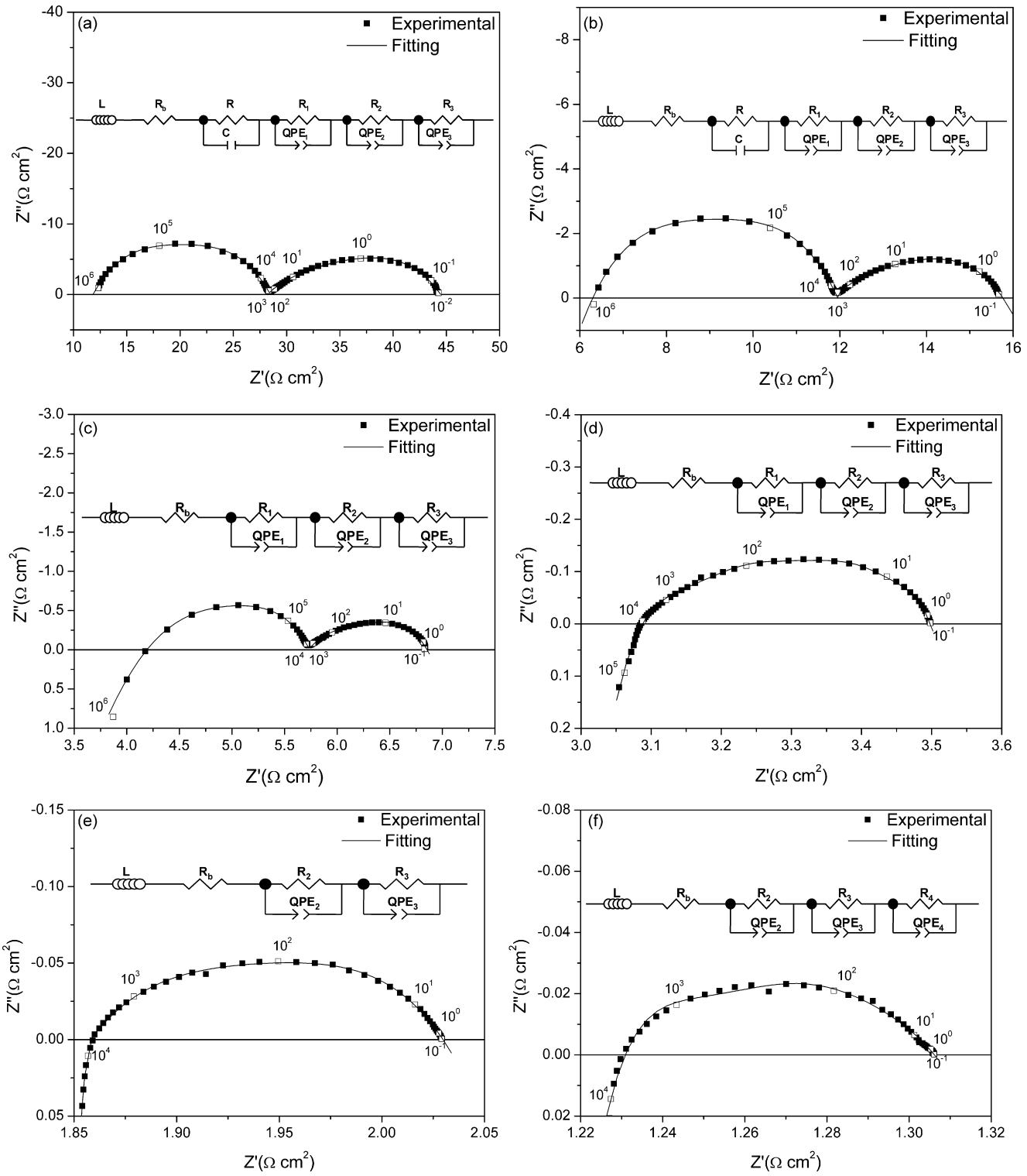

Fig. 4. Experimental and fit Nyquist plots for a symmetrical $PrBaCo_2O_{5+\delta}$/SDC/$PrBaCo_2O_{5+\delta}$ cell measured at open circuit in air: (a) 450 °C; (b) 500 °C; (c) 550 °C; (d) 600 °C; (e) 650 °C; (f) 700 °C. The equivalent circuits adopted for fitting the EIS data are inside the Nyquist plots.

range can be fitted based on the impedance of (R–C), composed of a resistor (R) in parallel with an ideal capacitor (C). The derived capacitance was found to be 2.11×10^{-7} F cm^{-2}, which agrees with the reported values for grain boundaries of SDC electrolytes [32]. With higher operation temperature, the size of this arc decreased. It totally disappeared above 600 °C. The calculated Ea for this process is about 0.91 eV, similar to the reported activation energy for oxygen diffusion around SDC electrolyte grain boundaries [31,32]. This implies that the well-separated semi-circle in the EIS ultra-high-frequency range at 450–600 °C may be associated with oxide-ion transfer through SDC electrolyte grain boundaries.

The second semi-circles in the EIS data are contributed from oxygen reduction over the PrBC electrode. According to Adler et al. [33], impedance at high and intermediate frequencies is related to ion and electron transfer at the electrode, electrolyte, and collector/electrode interfaces, while the impedance at low frequencies

Table 1
The fitting parameters as a function of temperature for $PrBaCo_2O_{5+\delta}$/SDC/$PrBaCo_2O_{5+\delta}$ in air under zero *dc* bias conditions (standard deviations range from 0.2% to 15%).

	T (°C)	450	500	550	600	650	700
	L (H)	1.51×10^{-7}	3.31×10^{-7}	4.09×10^{-7}	4.85×10^{-7}	5.02×10^{-7}	5.25×10^{-7}
	R_b (Ω cm^2)	11.85	6.02	3.52	2.64	1.85	1.22
	R (Ω cm^2)	10.41	4.04	–	–	–	–
	C (F cm^{-2})	2.11×10^{-7}	1.87×10^{-7}	–	–	–	–
Arc1	R_1 (Ω cm^2)	6.03	1.81	2.17	0.44	–	–
	CPE_1-Q (F cm^{-2})	6.73×10^{-6}	4.09×10^{-6}	2.62×10^{-7}	4.22×10^{-7}	–	–
	CPE_1-n	0.77	0.87	0.98	1.04	–	–
	C_1 (F cm^{-2})	3.39×10^{-7}	6.71×10^{-7}	1.84×10^{-7}	7.24×10^{-7}	–	–
	F_1 (Hz)	77845.4	131076.3	398812.8	499607.6	–	–
Arc2	R_2 (Ω cm^2)	7.01	1.80	0.50	0.21	0.11	0.02
	CPE_2-Q (F cm^{-2})	1.96×10^{-2}	3.08×10^{-2}	4.71×10^{-2}	6.19×10^{-2}	6.92×10^{-2}	5.00×10^{-2}
	CPE_2-n	0.64	0.63	0.60	0.62	0.66	0.78
	C_2 (F cm^{-2})	6.33×10^{-3}	5.43×10^{-3}	4.03×10^{-3}	4.57×10^{-3}	5.42×10^{-3}	7.03×10^{-3}
	F_2 (Hz)	3.6	16.3	78.9	164.1	271.6	1042.1
Arc3	R_3 (Ω cm^2)	9.14	2.07	0.66	0.21	7.07×10^{-2}	5.84×10^{-2}
	CPE_3-Q (F cm^{-2})	2.96×10^{-2}	3.55×10^{-2}	3.82×10^{-2}	5.81×10^{-2}	1.03×10^{-2}	9.66×10^{-2}
	CPE_3-n	0.88	0.88	0.87	0.85	0.84	0.75
	C_3 (F cm^{-2})	2.45×10^{-2}	2.47×10^{-2}	2.15×10^{-2}	2.75×10^{-2}	4.05×10^{-2}	1.64×10^{-2}
	F_3 (Hz)	0.7	3.1	11.2	27.4	55.6	165.9
Arc4	R_4 (Ω cm^2)	–	–	–	–	–	1.19×10^{-3}
	CPE_4-Q (F cm^{-2})	–	–	–	–	–	56.27
	CPE_4-n	–	–	–	–	–	1.18
	C_4 (F cm^{-2})	–	–	–	–	–	85.03
	F_4 (Hz)	–	–	–	–	–	1.6
	ASR (Ω cm^2)	22.18	5.68	3.33	0.86	0.18	8.13×10^{-2}

is associated with non-charge transfer, such as oxygen surface exchange and gas-phase diffusion inside and outside the electrode layer. Constant phase element (CPE) represents a non-ideal capacitor, and the associated CPE-Q parameter indicates the CPE's similarity to a true capacitor, for which CPE-Q = 1. To get more insight into the mechanism of oxygen reduction over the PrBC electrode, the capacitance and angular relaxation frequency f, which is an independent parameter of sample geometric characteristics and is a very use tool to identify the oxygen reduction process, were calculated based on the following equations [34]:

$$C_i = \frac{(R_i Q_i)^{(1/n_i)}}{R_i} \quad (2)$$

$$f_i = \frac{(R_i Q_i)^{-(1/n_i)}}{2\pi} \quad (3)$$

Table 1 summarizes the fitting parameters as a function of temperature for PrBC/SDC/PrBC in air under zero *dc* bias conditions. It was observed that both f and capacitance for Arc1 were similar to the reported values for oxide-ion transfer through the electrolyte–electrode interface [34]. Therefore, Arc1 is assigned to the impedance associated with oxide-ion charge transfer through the interface between PrBC and SDC. The polarization resistance associated with this process is about 1/3–2/3 that of the total electrode oxygen reduction, suggesting the oxygen-ion charge transfer through the electrode–electrolyte interface played an important role in the overall oxygen reduction in the PrBC electrode.

The angular relaxation frequency and capacitance of Arc2 and Arc3 is between 10^3–10^{-1} Hz and 10^{-2}–10^{-3} F cm^{-2}, respectively. Both are in the typical range for an electron charge transfer process [35]. The capacitance associated with the small arc (Arc4) in the low frequency range of the Nyquist plots (at operating temperature 700 °C) reaches 85 F cm^{-2}. Such a large capacitance is unlikely to be from any electrochemical process; it was therefore assigned to gas phase diffusion according to literature results [33,35].

To get more insight into the oxygen reduction at the cathode/electrolyte interface, a study of the influence of oxygen partial pressure and temperature on the electrode impedance was conducted. It is well known that different processes for oxygen reduction over mixed oxygen-ionic and electronic conducting electrodes have different relationships with the oxygen partial pressure. The most commonly used parameter to determine the rate-determining step in oxygen reduction process is m, which indicates the relation between the electrode resistance and oxygen partial pressure [34,35], as expressed by Eq. (4):

$$\frac{1}{R_p} = pO_2^m \quad (4)$$

The m value is 1, 0.5 and 0.25 for the rate-determining step as the adsorption of molecular oxygen at the electrode surface ($O_2(g) \Leftrightarrow O_{2,ads}$), the dissociation of molecular oxygen to atomic oxygen ($O_{2,ads} \Leftrightarrow 2O_{ads}$), and the electron transfer at the electrode/current-collector interface ($O_{2,ads} + 4e^- + 2V_O^{oo} \Leftrightarrow 2O_O^x$), respectively. Since the first semi-circle in EIS is contributed from the electrolyte, and the ionic conductivity of SDC is constant within the oxygen partial pressure of 0.04–1.0 atm, R_b was set to be a constant in the whole oxygen partial pressure range investigated when fitting the EIS data. Representative profiles for pO_2 dependence of R_1, R_2, R_3 and $R_2 + R_3$ are shown in Fig. 5 and the fitting results at 550 °C are listed in Table 2. It is clear that R_1 did not have a monotonic dependence on oxygen partial pressure. In some cases, R_1 even slightly decreased with decreasing pO_2. Such phenomena agree well with the characteristics of oxygen-ion transfer through the electrode–electrolyte interface. Polarization resistance of the oxygen-ion transfer through the electrolyte–electrode interface is closely related to oxygen-ionic conductivity of both the electrolyte and electrode. As mentioned above, the SDC electrolyte is independent of the oxygen partial pressure within the investigated pressure range (0.04–1 atm). The oxygen-ionic conductivity of a mixed conductor is closely related with the oxygen vacancy concentration in the oxide lattice since oxygen vacancies are the charge carrier of oxygen-ions. It is observed that lattice oxygen can be released from PrBC with decreasing oxygen partial pressure or increasing the temperature [19]. This implies that the oxygen-ionic conductivity may be improved with decreasing oxygen partial pressure. This explains the slight increase in R_1 with decreasing oxygen partial pressure at some temperatures.

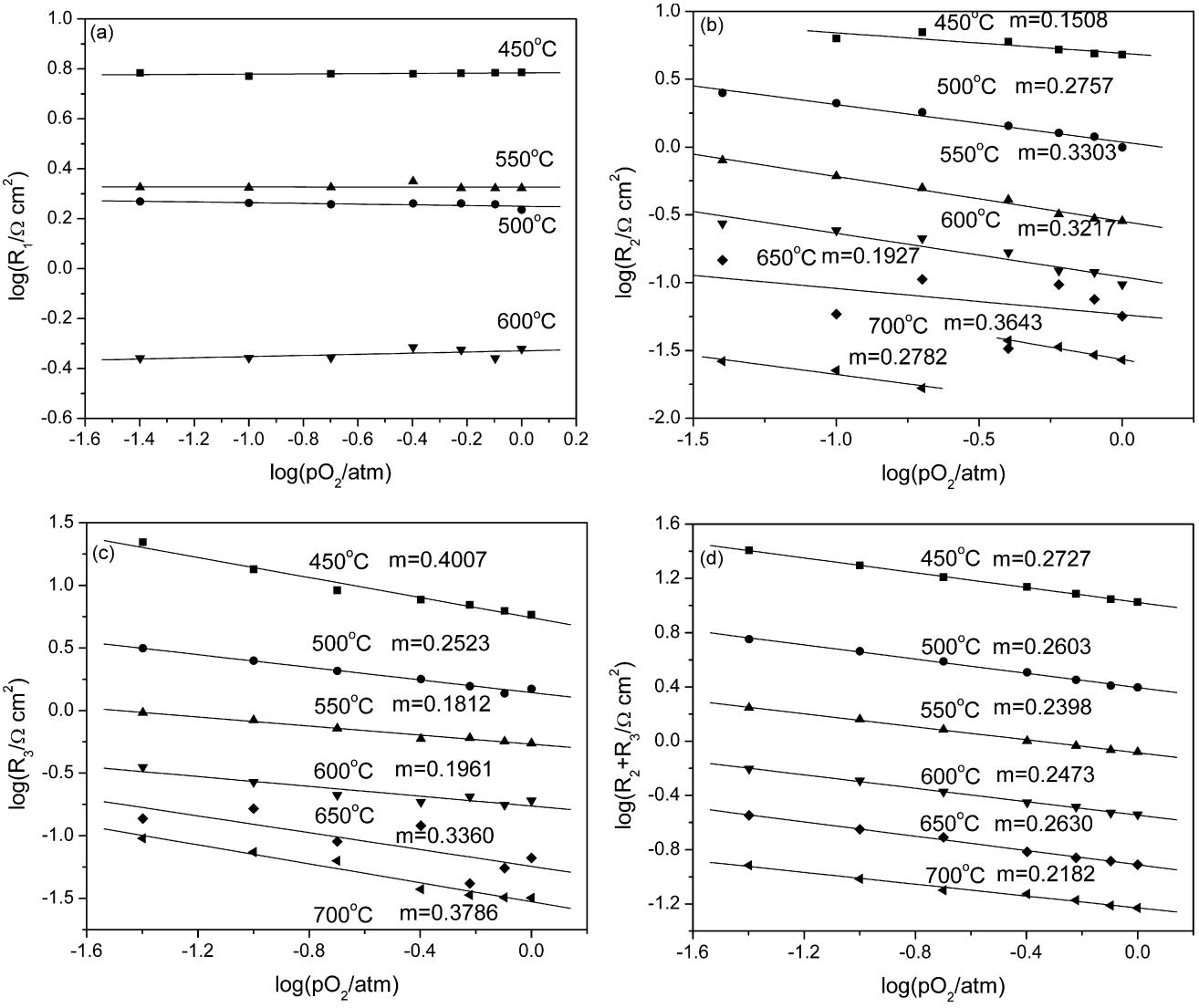

Fig. 5. Representative profiles for pO_2 dependence of (a) R_1, (b) R_2, (c) R_3 and (d) $(R_2 + R_3)$.

Table 2
The fitting results of $PrBaCo_2O_{5+\delta}$/SDC/$PrBaCo_2O_{5+\delta}$ as a function of oxygen partial pressure at 550 °C (standard deviations range from 0.2% to 15%).

	P (atm)	0.04	0.1	0.2	0.4	0.6	0.8	1
	L (H)	4.77×10^{-7}	4.80×10^{-7}	4.84×10^{-7}	3.98×10^{-7}	4.74×10^{-7}	4.60×10^{-7}	4.80 × 10-7
	R_b (Ω cm^2)	3.65	3.65	3.65	3.51	3.65	3.65	3.65
Arc1	R_1 (Ω cm^2)	2.11	2.11	2.11	2.24	2.10	2.10	2.10
	CPE_1-Q (F cm^{-2})	2.92×10^{-7}	3.09×10^{-7}	3.12×10^{-7}	2.82×10^{-7}	2.94×10^{-7}	2.80×10^{-7}	2.94×10^{-7}
	CPE_1-n	0.97	0.97	0.97	0.97	0.97	0.98	0.97
	C_1 (F cm^{-2})	1.89×10^{-7}	1.90×10^{-7}	1.89×10^{-7}	1.81×10^{-7}	1.91×10^{-7}	1.94×10^{-7}	1.91×10^{-7}
	F_1 (Hz)	398593.9	396254.9	399167.8	393408.6	396287.7	391966.5	397124.1
Arc2	R_2 (Ω cm^2)	0.80	0.61	0.50	0.41	0.32	0.30	0.28
	CPE_2-Q (F cm^{-2})	5.27×10^{-2}	5.21×10^{-2}	5.37×10^{-2}	5.11×10^{-2}	5.64×10^{-2}	5.54×10^{-2}	5.51×10^{-2}
	CPE_2-n	0.62	0.60	0.59	0.57	0.55	0.54	0.54
	C_2 (F cm^{-2})	7.84×10^{-3}	5.42×10^{-3}	4.18×10^{-3}	2.91×10^{-3}	2.08×10^{-3}	1.67×10^{-3}	1.52×10^{-3}
	F_2 (Hz)	25.4	48.1	76.3	133.7	239.0	322.7	368.5
Arc3	R_3 (Ω cm^2)	0.96	0.84	0.72	0.59	0.60	0.56	0.55
	CPE_3-Q (F cm^{-2})	4.83×10^{-2}	4.06×10^{-2}	3.90×10^{-2}	3.50×10^{-2}	3.23×10^{-2}	3.08×10^{-2}	3.07×10^{-2}
	CPE_3-n	0.88	0.87	0.84	0.83	0.80	0.80	0.79
	C_3 (F cm^{-2})	3.22×10^{-2}	2.40×10^{-2}	2.00×10^{-2}	1.61×10^{-2}	1.22×10^{-2}	1.11×10^{-2}	1.02×10^{-2}
	F_3 (Hz)	5.1	7.9	11.1	16.6	21.7	25.5	28.4
	ASR (Ω cm^2)	3.87	3.56	3.33	3.24	3.02	2.96	2.93

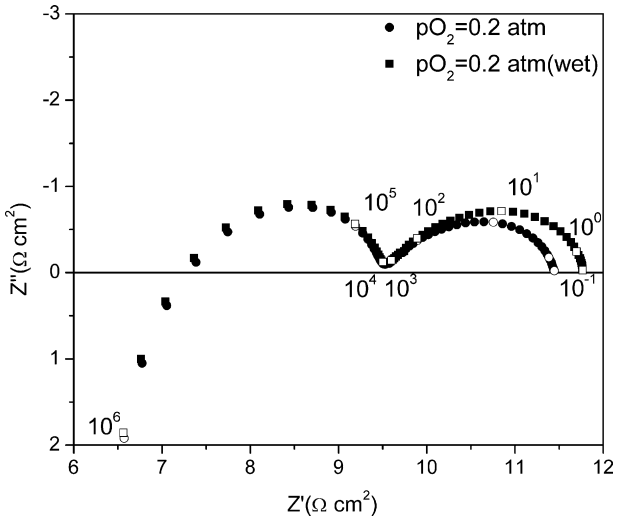

Fig. 6. Typical EIS of a symmetric $PrBaCo_2O_{5+\delta}$/SDC/$PrBaCo_2O_{5+\delta}$ cell measured at 550 °C with and without the water vapor (3 vol.%) while fixing the oxygen partial pressure at 0.2 atm.

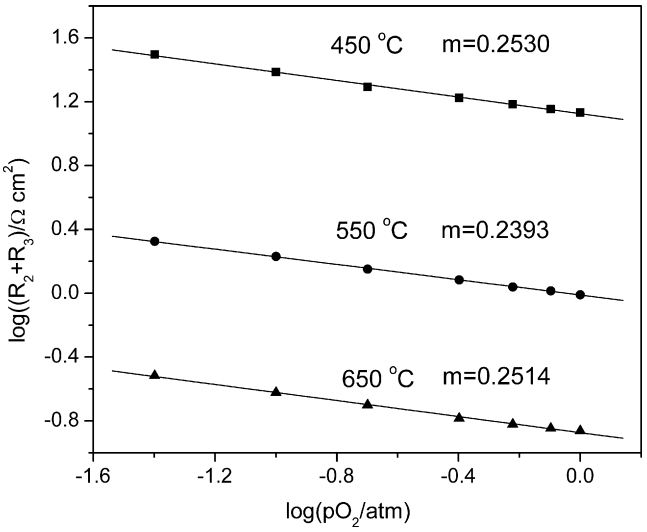

Fig. 7. The m value derived from the oxygen partial pressure dependence of $R_2 + R_3$ when water vapor was introduced into the atmosphere.

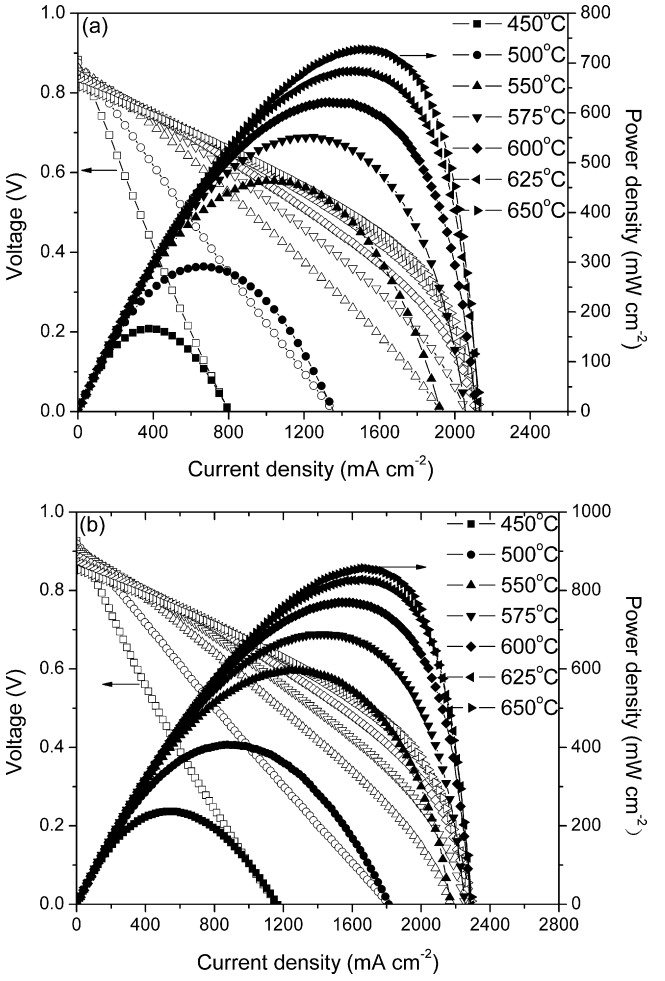

Fig. 8. The *I–V* curves of the cell with an electrolyte thickness of ~20 μm at various temperatures between 450 and 650 °C with (a) air and (b) oxygen as the cathode atmosphere and hydrogen as the anode fuel.

Table 3
The corresponding fitting results of the typical EIS of the symmetric cell measured as a function of oxygen partial pressure at 550 °C, with the water vapor (3 vol.%) introduced (standard deviations range from 0.2% to 15%).

	P (atm)	0.04	0.1	0.2	0.4	0.6	0.8	1
	L (H)	4.73×10^{-7}	4.71×10^{-7}	4.71×10^{-7}	4.65×10^{-7}	4.72×10^{-7}	4.82×10^{-7}	4.71×10^{-7}
	R_b (Ω cm^2)	3.65	3.65	3.65	3.65	3.65	3.65	3.65
Arc1	R_1 (Ω cm^2)	2.13	2.14	2.12	2.11	2.12	2.12	2.11
	CPE_1-Q (F cm^{-2})	3.10×10^{-7}	3.22×10^{-7}	3.19×10^{-7}	3.16×10^{-7}	3.15×10^{-7}	3.15×10^{-7}	3.07×10^{-7}
	CPE_1-n	0.97	0.96	0.97	0.97	0.97	0.97	0.97
	C_1 (F cm^{-2})	1.90×10^{-7}	1.90×10^{-7}	1.91×10^{-7}	1.94×10^{-7}	1.92×10^{-7}	1.91×10^{-7}	1.93×10^{-7}
	F_1 (Hz)	393720.0	391207.0	391958.6	389588.5	391800.1	393575.4	391368.8
Arc2	R_2 (Ω cm^2)	0.86	0.691	0.57	0.40	0.36	0.32	0.33
	CPE_2-Q (F cm^{-2})	5.85×10^{-2}	5.31×10^{-2}	5.20×10^{-2}	5.99×10^{-2}	5.69×10^{-2}	5.70×10^{-2}	5.71×10^{-2}
	CPE_2-n	0.61	0.61	0.60	0.55	0.55	0.54	0.54
	C_2 (F cm^{-2})	8.86×10^{-3}	6.19×10^{-3}	4.89×10^{-3}	2.97×10^{-3}	2.52×10^{-3}	1.85×10^{-3}	2.06×10^{-3}
	F_2 (Hz)	20.9	37.3	56.7	133.2	174.6	270.0	231.5
Arc3	R_3 (Ω cm^2)	1.25	1.01	0.84	0.81	0.73	0.72	0.65
	CPE_3-Q (F cm^{-2})	4.59×10^{-2}	3.93×10^{-2}	3.74×10^{-2}	3.14×10^{-2}	3.02×10^{-2}	2.85×10^{-2}	2.98×10^{-2}
	CPE_3-n	0.87	0.87	0.86	0.82	0.81	0.80	0.80
	C_3 (F cm^{-2})	2.99×10^{-2}	2.47×10^{-2}	2.12×10^{-2}	1.40×10^{-2}	1.26×10^{-2}	1.08×10^{-2}	1.14×10^{-2}
	F_3 (Hz)	4.2	6.4	8.9	14.0	17.3	20.5	21.7
	ASR (Ω cm^2)	4.24	3.84	3.54	3.32	3.21	3.15	3.09

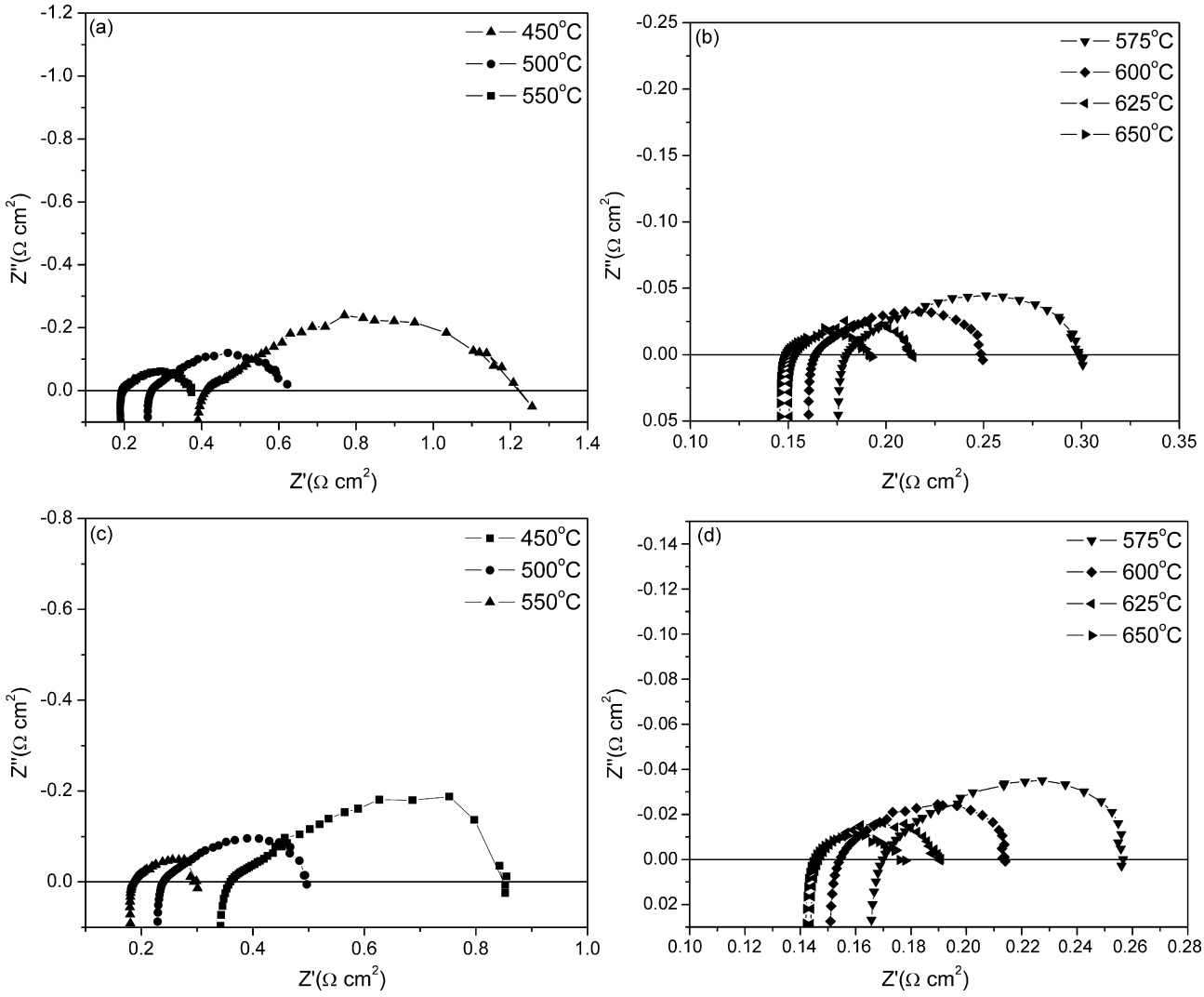

Fig. 9. Nyquist plots for the corresponding EIS of a single cell under OCV conditions with (a, b) air and (c, d) oxygen as the cathode atmosphere at various operating temperatures.

The polarization resistances R_2 and R_3, associated with Arc2 and Arc3 appearing at intermediate frequency ranges, were found to be highly dependent on oxygen partial pressure. Both R_2 and R_3 decreased with increased oxygen partial pressure. The values obtained for m were 0.15–0.4 for both R_2 and R_3 at the investigated temperatures. $R_2 + R_3$ was found to be dependent on pO_2 with the value $m \sim 0.25$. It suggests that both R_2 and R_3 are associated with electron transfer. In other word, the electron transfer process may be composed of two successive intermediate steps, showing comparable importance in the charge transfer process. At 700 °C, the additional arc (Arc4) in the low frequency range disappeared with increasing oxygen partial pressure. This suggests that the polarization resistance of this process quickly reduced with increasing oxygen partial pressure, which is in agreement with the behavior of a gas diffusion process. An increase of oxygen partial pressure results in a sufficient supply of oxygen to the electrode from the gas phase thereby effectively eliminating diffusion polarization resistance.

To further support above oxygen reduction mechanism, some water vapor (3 vol.%) was introduced intentionally into the surrounding atmosphere while keeping the oxygen partial pressure constant. The influence of water on oxygen reduction may include: competitive adsorption of water over the active electrode sites for oxygen adsorption and blocking oxygen diffusion by adsorbing on the oxygen passage. Both of these processes could have a detrimental effect on oxygen reduction. On the other hand, water can also join in oxygen dissociation or charge transfer processes and alter the oxygen reduction route via the following reactions [36,37]:

$$H_2O(g) \Leftrightarrow H_2O_{ad} \quad (5)$$

$$\tfrac{1}{2}O_2(g) \Leftrightarrow O_{ad} \quad (6)$$

$$H_2O_{ad} + O_{ad} + 2e^- \Leftrightarrow 2OH'_{ad} \quad (7)$$

$$H_2O(g) + O^{2-} \Leftrightarrow 2OH'_{ad} \quad (8)$$

$$2OH'_{ad} \Leftrightarrow O^{2-} + H_2O_{ad} \quad (9)$$

$$H_2O_{ad} \Leftrightarrow H_2O(g) \quad (10)$$

Because of the high oxygen partial pressure, proton conductivity is reasonably assumed to be negligible. Therefore, the introduction of water vapor should have negligible effects on the bulk oxygen-ionic conductivity of the electrode. This implies that R_2, which is associated with oxygen-ion charge transfer through the electrolyte–electrode interface, should remain constant even with the introduction of water vapor.

Fig. 6 shows typical EIS results for a symmetric cell measured at 550 °C, with and without the water vapor (3 vol.%) while fixing the oxygen partial pressure at 0.2 atm. The introduction of

water vapor into the atmosphere resulted in a greater impedance, with lower temperatures showing more significant increments. Corresponding fitting results are listed in Table 3. The R_1 value remained unchanged with the introduction of water vapor, which agrees well with the characteristics of oxygen transfer through the electrode–electrolyte interface. The m value derived from the oxygen partial pressure dependence of $R_2 + R_3$ was still ~0.25 after the water vapor was introduced, as shown in Fig. 7. This suggests that reduction mechanism was not altered by the introduction of water vapor. The impedance increment with water vapor could then be associated with competitive occupation of oxygen adsorption sites. Since water adsorption is more severe at lower temperatures, this then explains the increased effect of water vapor on polarization resistance of $R_2 + R_3$ at lower temperatures.

Based on above analysis, it is clear that oxygen reduction over the PrBC cathode is mainly from the charge transfer process, including both oxygen-ion transfer from the electrode to the electrolyte layer across the electrode–electrolyte interface and the electron transfer over the electrode surface.

3.3. Single cell performance

Ni + SDC anode-supported thin-film SDC electrolyte fuel cells were fabricated to evaluate the performance of PrBC electrode in real fuel cell operation conditions. A firing temperature of 1000 °C was adopted for the PrBC cathode layer. Fig. 8a shows the *I–V* curves of the cell with an electrolyte thickness of ~20 μm at various temperatures between 450 and 650 °C while applying air as the cathode atmosphere and hydrogen as the anode fuel. High power densities were achieved. For example, at an operating temperature of 600 °C, the peak power density reached ~620 mW cm^{-2}, only modestly lower than that of a similar fuel cell with a perovskite-type BSCF cathode, which has shown outstanding cathode performance for oxygen reduction at reduced temperature [9]. Fig. 9 shows Nyquist plots for the corresponding EIS of a single cell under OCV condition at various operating temperatures. The polarization resistances presented here are a sum of the cathode and anode polarization resistances. As compared to the results from symmetric cell test, the electrode polarization resistances of the single cell under an asymmetric atmosphere of air versus hydrogen are even smaller. For example, the sum of the cathodic and anodic polarization resistance measured by the single cell is around 0.1 Ω cm^2 while the polarization resistance measured by a symmetric cell configuration is 0.4 Ω cm^2 at 600 °C. This suggests that the cathode performance improved under these fuel cell operational conditions. Based on the results in Fig. 9, the cell resistance at 600 °C was mainly due to ohmic loss of the electrolyte. It suggests that tailoring the thickness of electrolyte may lead to significantly improved cell performance. On the other hand, while decreasing the thickness of electrolyte, the extent of internal shorting in the cell should be considered [38]. Fig. 8b and Fig. 9c and d are *I–V* curves and corresponding EIS under OCV conditions at various temperatures when applying oxygen as the cathode atmosphere, respectively. Compared to the results by applying air as the cathode atmosphere, the performances improved only slightly when oxygen was selected. It further confirms that the main electrical loss is from the electrolyte.

As compared to the fuel cell with a BSCF cathode [9], deterioration in cell performance with decreasing temperature is much slower for the fuel cell with a PrBC cathode. For example, a reported peak power density of 1010 and 180 mW cm^{-2} was achieved for the cell with BSCF cathode at 600 and 445 °C, respectively [9]. It corresponds to a fivefold loss in power density when the temperature decreased from 600 to 450 °C. For a cell with a PrBC cathode, the corresponding peak power densities are 620 and 165 mW cm^{-2}, respectively, or a three fold reduction. The above results suggest that PrBC may be more suitable for low-temperature operation. Such characteristics agree well with the high oxygen activity of PrBC at reduced temperatures [21].

4. Conclusions

With an aim of developing high-performance intermediate-temperature solid-oxide fuel cells, the mixed ionic and electronic conducting A-site cation-ordered $PrBaCo_2O_{5+\delta}$ (PrBC) oxide has been investigated as the cathode on a samarium-doped ceria (SDC) electrolyte. The phase reaction between PrBC and SDC was demonstrated not serious even at 1100 °C. An EDTA–citrate sol–gel synthesis of the powder fired at 1000 °C can attach the cathode to the electrolyte surface very well without serious reactions between the two layers. Based on a symmetric configuration, an area specific polarization resistance of ~0.40 Ω cm^2 at 600 °C in air was achieved, which is comparable to literature results. It demonstrated the potential application of PrBC as a cathode for IT-SOFCs. The impendance's relationship to oxygen partial pressure and water vapor demonstrated that oxygen reduction on PrBC electrode was rate-determined mainly by oxygen-ion charge transfer through the electrolyte–electrode interface and electron transfer over the electrode surface, which was possibly composed of two successive steps. Under single cell conditions, the main polarization resistance of the cell was from the electrolyte ohmic drop. Under optimal conditions, a peak power density of ~620 mW cm^{-2} at 600 °C was achieved for an anode-supported cell using a PrBC cathode. Considering favorable oxygen reduction and electronic conductivity conditions, PrBC may be a highly promising cathode material for IT-SOFC based on doped ceria electrolytes.

Acknowledgements

This work was supported by the National Natural Science Foundation of China under contract Nos. 20676061 and 20703024, by the National 863 program under contract No. 2007AA05Z133, and by the National Basic Research Program of China under contract No. 2007CB209704. Dr. Zongping Shao also acknowledges financial support from the Chinese Ministry of Education via the Program for Changjiang Scholars and Innovative Research Teams at Universities (No. IRT0732).

References

[1] B.C.H. Steele, A. Heinzel, Nature 414 (2001) 345–352.
[2] N.P. Brandon, S. Skinner, B.C.H. Steele, Annu. Rev. Mater. Res. 33 (2003) 183–213.
[3] S.C. Singhal, K. Kendall, High-temperature Solid Oxide Fuel Cells: Fundamentals, Design and Applications, Elsevier Advanced Technology, UK, 2003.
[4] N.Q. Minh, J. Am. Ceram. Soc. 76 (1993) 563–588.
[5] J.E.H. Sansom, E. Kendrick, H.A. Rudge-Pickard, M.S. Islam, A.J. Wright, P.R. Slater, J. Mater. Chem. 15 (2005) 2321–2327.
[6] J. Wan, J.B. Goodenough, J.H. Zhu, Solid State Ionics 178 (2007) 281–286.
[7] K.T. Lee, A. Manthiram, Chem. Mater. 18 (2006) 1621–1626.
[8] C.R. Xia, W. Rauch, F.L. Chen, M.L. Liu, Solid State Ionics 149 (2002) 11–19.
[9] Z.P. Shao, S.M. Haile, Nature 431 (2004) 170–173.
[10] J. Pena-Martinez, D. Marrero-Lopez, D. Perez-Coll, J.C. Ruiz-Morales, P. Nunez, Electrochim. Acta 52 (2007) 2950–2958.
[11] K.K. Hansen, K.V. Hansen, Solid State Ionics 178 (2007) 1379–1384.
[12] K.K. Hansen, M. Sogaard, M. Mogensen, Electrochem. Solid State Lett. 10 (2007) B119–B121.
[13] S. Bebelis, N. Kotsionopoulos, A. Mai, F. Tietz, J. Appl. Electrochem. 37 (2007) 15–20.
[14] K.T. Lee, A. Manthiram, J. Electrochem. Soc. 153 (2006) A794–A798.
[15] J.M. Ralph, C. Rossignol, R. Kumer, J. Electrochem. Soc. 150 (2003) A1518–A1522.
[16] A.A. Taskin, A.N. Lavrov, Y. Ando, Prog. Solid State Chem. 35 (2007) 481–490.
[17] G. Kim, S. Wang, A.J. Jacobson, Z. Yuan, W. Donner, C.L. Chen, L. Reimus, P. Brodersen, C.A. Mims, Appl. Phys. Lett. 88 (2006) 024103.
[18] A.A. Taskin, A.N. Lavrov, Y. Ando, Appl. Phys. Lett. 86 (2005) 091910.
[19] C. Frontera, A. Caneiro, A.E. Carrillo, J. Oro-Sole, J.L. Garcia-Munoz, Chem. Mater. 17 (2005) 5439–5445.
[20] A. Tarancon, S.J. Skinner, R.J. Chater, F. Hernandez-Ramirez, J.A. Kilner, J. Mater. Chem. 17 (2007) 3175–3181.
[21] G. Kim, S. Wang, A.J. Jacobson, L. Reimus, P. Brodersen, C.A. Mims, J. Mater. Chem. 17 (2007) 2500–2505.

[22] B. Lin, S.Q. Zhang, L.C. Zhang, L. Bi, H.P. Ding, X.Q. Liu, J.F. Gao, G.Y. Meng, J. Power Sources 177 (2008) 330–333.
[23] N. Li, Z. Lu, B. Wei, X.Q. Huang, K.F. Chen, Y.H. Zhang, W.H. Su, J. Alloys Compd. 454 (2008) 274–279.
[24] A. Tarancon, A. Morata, G. Dezanneau, S.J. Skinner, J.A. Kilner, S. Estrade, F. Hernandez-Ramirez, F. Peiro, J.R. Morante, J. Power Sources 174 (2007) 255–263.
[25] A.M. Chang, S.J. Skinner, J.A. Kilner, Solid State Ionics 177 (2006) 2009–2011.
[26] J.H. Kim, A. Manthiram, J. Electrochem. Soc. 155 (2008) B385–B390.
[27] W. Zhou, Z.P. Shao, W.Q. Jin, J. Alloys Compd. 426 (2006) 368–374.
[28] H.X. Gu, R. Ran, W. Zhou, Z.P. Shao, J. Power Sources 172 (2007) 704–712.
[29] C.J. Zhu, X.M. Liu, C.S. Yi, D.T. Yan, W.H. Su, J. Power Sources 185 (2008) 193–196.
[30] A. Mitterdorfer, L.J. Gauckler, Solid State Ionics 111 (1998) 185–218.
[31] Z.L. Zhan, T.L. Wen, H.Y. Tu, Z.Y. Lu, J. Electrochem. Soc. 148 (2001) A427–A432.
[32] V. Esposito, E. Traversa, J. Am. Ceram. Soc. 91 (2008) 1037–1051.
[33] S.B. Adler, X.Y. Chen, J.R. Wilson, J. Catal. 245 (2007) 91–109.
[34] M.J. Escudero, A. Aguadero, J.A. Alonso, L. Daza, J. Electroanal. Chem. 611 (2007) 107–116.
[35] Y. Takeda, R. Kanno, M. Noda, Y. Tomida, O. Yamamoto, J. Electrochem. Soc. 134 (1987) 2656–2661.
[36] N. Sakai, K. Yamaji, T. Horita, Y.P. Xiong, H. Kishimoto, M.E. Brito, H. Yokokawa, Solid State Ionics 176 (2005) 2327–2333.
[37] N. Sakai, K. Yamaji, T. Horita, H. Kishimoto, Y.P. Xiong, H. Yokokawa, Solid State Ionics 175 (2004) 387–391.
[38] X.G. Zhang, M. Robertson, C. Deces-Petit, W. Qu, O. Kesler, R. Maric, D. Ghosh, J. Power Sources 164 (2007) 668–677.